Phase equilibria and thermodynamic evaluation of the Fe-Ti-V-O system in air

Willem Dutoit Malan[a], Guven Akdogan[b], Pekka Taskinen[c], Johan Zietsman[a]

[a]*Department of Material Sciences and Metallurgical Engineering, University of Pretoria, Private Bag X20, Hatfield, 0028, South Africa*
[b]*Department of Process Engineering, Stellenbosch University, Banghoek Rd, 7599, South Africa*
[c]*Metallurgical Thermodynamics and Modelling, School of Chemical Engineering, Aalto Unviersity Vuorimiehentie 2K, FI-00076 Aalto*

Abstract

In this study, the iron-titanium-vanadium-oxygen (Fe-Ti-V-O) system in equilibrium with air was studied experimentally by high-temperature equilibration, quenching, scanning electron microscope and microprobe analysis coupled with critical assessment and thermodynamic evaluation. The properties of the liquid phase were successfully described with the quasichemical model by optimizing parameters only related to the Fe-Ti-O system; remaining parameters for the Fe-V-O and Ti-V-O sub-systems were adopted from recent optimisations. The model for the rutile and hematite solid solutions were described with the compound energy formalism. The ferropseudobrookite solid solution was modelled with a simple polynomial model to include a small solubility V_2O_5. A final set of self-consistent thermodynamic parameters was estimated within acceptable error limits. Calculated isothermal projections at 1000 °C, 1100 °C, 1200 °C, 1300 °C, and 1400 °C of the Fe-Ti-V-O system in equilibrium with air are presented and compared to experimental observations.

Key words: Fe-Ti-V-O system, thermodynamics, static experiments, phase diagram

1. Introduction

In two earlier studies, [1, 2] the Fe-V-O and Ti-V-O systems in air were investigated and their technological importance was explained. These two systems were studied experimentally in temperatures ranging from 700 °C to 1500 °C and a set of self-consistent thermodynamic parameters was estimated. The calculated phase diagrams of the studied systems were presented and compared to experimental observations and other phase diagram data from literature. The lower-order Fe-Ti-O system has been the subject of many previous investigations and have been included in the FToxid database of FactSage [3, 4]. However, experimental investigations and thermodynamic assessments of this system were limited mostly to reducing conditions, thereby compromising accurate equilibrium estimations with FactSage under oxidising conditions [5].

Although previous studies have been conducted on the Fe-Ti-V-O system in air, most were done with dynamic equilibration techniques (e.g. differential scanning calorimetry (DSC), differential thermal analysis (DTA), thermogravimetric analysis (TGA)), of which the recording accuracy relies heavily on fast phase transformations [6]. Many oxide systems have sluggish transport kinetics, and consequently dynamic techniques can produce spurious results. This is due to the sample not being at equilibrium due to the dynamic nature of the techniques. The equilibration-quench analysis experimental technique is static by nature and emulates a system that is near or at equilibrium [7].

Knowing that equilibrium is preserved, static experiments were carried out between 1000 °C and 1400 °C to characterise phase assemblages, and study phase transformation in the higher order Fe-Ti-V-O system in air. The data were used to optimise parameters of thermodynamic models capable of estimating phase equilibrium from a given elemental composition and temperature under oxidising conditions. Some added advantages that support the need for experimentally determined liquidus and solidus compositions of the studied system include: better indication of which ternary interpolation technique should be used; confirmation of no intermediate ternary compounds; confirmation whether any ternary terms are necessary to reproduce experimental phase diagram data within acceptable error limits [8]. The thermodynamic evaluation was performed with FactSage 7.0 [5].

Although the higher order Fe-Ti-V-O system in air can not be linked directly to a mineral process such as the extraction of vanadium from a titaniaferous magnetite concentrate. The latter involves carbothermic reduction of a

pre-reduced titaniaferous magnetite concentrate, followed by the oxidation of the liquid metal through a shaking ladle process. The shaking ladle process follows a soft oxygen blowing practice where reactions take place at a temperature below 1400 °C [9]. Detailed information about phase equilibria (e.g. liquidus temperatures) of the V-Al-Ca-Fe-Na-Ti-Si-O system, especially in the shaking ladle process where reactions take place fast and under reducing conditions, is essential to understand how vanadium distributes among phases. Therefore, for the system to become applicable to this process and other processes used to treat vanadium-containing metallurgical slag, more work needs to be done under reducing conditions. The results from this study can then be combined with results from such studies to expand databases such as the FToxid database in order to estimate the thermochemical behaviour of vanadium-containing oxide systems in FactSage.

2. Literature Data

2.1. Structure and Phase Transformation

Structures and phase transformation of compounds in the lower-order Fe-V-O and Ti-V-O phase regions were discussed in our previous studies [1, 2].

Pseudo-brookite solid solution or solid compound, Fe_2TiO_5(s), has been show to exist in the Fe-Ti-O system in air [10, 11]. In these studies, the ternary compound was shown to decompose into its respective binary oxides, Fe_2O_3 and TiO_2 at 565±15 °C. Guo et al. [12] had investigated the crystal structure by means of x-ray diffraction (XRD), Mössbauer spectroscopy and neutron diffraction. The results confirmed that the $Fe_{1+x}Ti_{2-x}O_5$ ferropseudobrookite solid solution has an orthorhombic structure with D_{2h}^{17}(Cmcm) spacegroup. In their work they also showed that site occupancies obtained from both Mössbauer spectra and neutron diffraction data indicated that the cation (Fe^{2+}, Fe^{3+} and Ti^{4+}) distributions in the available sites, 4c and 8f, are neither random nor perfectly ordered. The compound, Fe_2TiO_5(s), melts congruently at 1388 °C. However, this congruent melting point is estimated with FactSage and has not been determined experimentally.

2.2. Liquidus and solidus data

Sub-solidus experimental data of the system exist up to 700 °C. Fotiev et al. [6] investigated compatibility relations among crystalline phases for ternary combinations of Fe_2O_3, TiO_2 and V_2O_5 in air. Two vanadate compounds have been reported between Fe_2O_3 and V_2O_5, namely $FeVO_4$ (orthovanadate) and $Fe_2V_4O_{13}$. No ternary compounds were observed and no intermediate compounds were detected in the V_2O_5 and TiO_2 subsystem in air. All samples were heat-treated below the liquidus temperature. No liquidus data of the Fe-Ti-V-O system under oxidising conditions were found in literature. The Fe-V-O and Ti-V-O systems in air were evaluated thermodynamically in our previous two studies [1, 2]. The Fe-Ti-O system is available in FactSage, but has not been evaluated under oxidising conditions.

It has been reported in the description of the FToxid database that slags containing Fe_2O_3 and TiO_2 have not been evaluated. As a result, calculations can only be made with the FToxid database under reducing conditions where Fe is mainly present as Fe^{2+}, although reasonable calculations of the Fe^{3+} content can be obtained as long as the Fe^{3+} content is low. However, the calculations in the present study were performed in air and Fe^{3+} is known to be the dominant valance of iron under these conditions [5].

Furthermore, it is reported in the FToxid database that the model for ferropseudobrookite solid solution may only be used under relatively reducing conditions [5]. Fe_2O_3 is not a component of the ferropseudobrookite solid solution in the model. Therefore, any calculations of the Fe-Ti-O system under oxidizing conditions excludes Fe_2O_3. The model was developed within the framework of the compound energy formalism by Erikson et al. [4], in which the solution of $FeTi_2O_5$ and Ti_3O_5 was represented as $(Fe^{2+}_{1-x}, Ti^{3+}_x)(Ti^{4+}_{2-x}, Ti^{3+}_x)$, with the ions mixing randomly on each site. The model successfully reproduced experimental results under reducing conditions.

To our knowledge, no experimental or theoretical data of the ferropseudobrookite solid solution under oxidizing conditions have been reported. For this reason, the dissolution of TiO_2(s) and Fe_2O_3(s) in ferropseudobrookite solid solution under oxidizing conditions cannot be reproduced with the available model and data in FactSage.

2.3. Thermodynamic data

The enthalpies of formation, standard entropies and heat capacities of $FeVO_4$(s) and $Fe_2V_4O_{13}$(s) were obtained from our previous study on the Fe-V-O system in air. All thermodynamic data of other compounds in the Fe-Ti-V-O system were taken from the FactPS database [5], unless otherwise stated.

$FeTi_2O_5$(s) is not in the FToxid database, but inside the FactPS database of FactSage means that its thermodynamic properties were never properly assessed. Therefore, it would not have been prudent to simply copy the properties and put the reference to FactSage. The free energy of formation of $FeTi_2O_5$(s) from Fe_2O_3(s) and TiO_2 between 700 and 1200 K, was measured and calculated by [11] as $\Delta G^{\circ}(T) = 1990 - 2.4T$ Cal (T in Kelvin). Properties such as enthalpy of formation and standard entropy were optimised to reproduce present experimental data within acceptable error limits. This is because of the partial dissolution of V_2O_5(s) in $FeTi_2O_5$(s) observed in subsection 6.1 (ferricpseudobrookite solid solution).

No other thermodynamic experimental data, such as enthalpies of mixing, thermal expansion data, heat contents and activity data of the slag phase, were found in literature, which highlights the need for further experimental work.

3. Experiments

3.1. Sample Preparation

The starting materials used for the experiments were V_2O_5(s), TiO_2(s) and Fe_2O_3(s). The material, source and purity are presented in Table 1. Mixtures of selected bulk compositions were prepared by weighing the oxide powders (< 0.5 g), followed by mixing them thoroughly using an agate mortar and pestle. The samples were pellitised to 20 Mpa.

Table 1: Purity of initial materials and sources from which they were acquired.

Material	Source	Purity
Divanadium Pentaoxide	SIGMA ALDRICH, RSA	99.60%
Ferric Oxide	SIGMA ALDRICH, RSA	>99 %
Anatase	SIGMA ALDRICH, RSA	99.90%

3.2. Experimental Procedure

The experimental procedure is similar to the procedures followed in our previous studies on the Fe-V-O and Ti-V-O systems in air [1, 2]. Nevertheless, a short description is given, pointing out the most important aspects.

All equilibration experiments were conducted in a vertical electrical resistance tube furnace (Lenton, UK) with a 35 mm inner diameter alumina work tube. The maximum operating temperature is 1600 °C. The first step involved in ascertaining a thermal profile of the furnace worktube to identify the hot zone in the tube furnace. The S-type thermocouples were calibrated according to the melting point of copper. A calibrated S-type thermocouple connected to a Keithley 2010 DMM multimeter (Cleveland, OH, USA) and a cold junction compensation was connected to a Keithley 2000 multi-meter (Cleveland, OH, USA) to measure the ambient temperature with a PT100 sensor (Platinum Resistance thermometer, SKS Group, Finland). The temperature was captured and logged every 2 seconds with a NI labVIEW temperature logging program. A small hot zone of 4 - 5 cm in length was established. The deviation of temperature measurements in the hot zone was less then 2 °C.

Attainment of equilibrium was achieved by comparing samples with identical starting composition at fixed time intervals to one another at constant temperature, and assessing compositional homogeneity of the phases with SEM-EDS and EPMA. Time interval experiments were done prior to experiments at different temperatures. Equilibrium at 1000 °C was achieved after 4 hours of equilibration and this was also the lowest temperature at which experiments were carried out. All specimens were lowered into the furnace with platinum (Pt) wire in a Pt envelope. Furthermore, SEM-EDS analysis showed that samples were not contaminated with Pt. Each experiment was repeated at least once.

Experiments in air were undertaken with the bottom of the tube furnace open and exposed to the atmosphere. The sample was introduced into the furnace from the bottom by slowly pulling on the wire from the top of the furnace. The slag behaved extremely aggressively, which was attributed to experimental temperatures being well above the melting temperature of V_2O_5 (669.85 °C). The melting point was determined with FactSage 7.0 [5]. This in turn caused a superheated V-O slag to form. A systematic increase in temperature was required to contain the aggressive slag. The specimen was allowed to melt slowly by keeping the sample in a lower temperature area of the furnace for 30 to 45 s before finally raising it into the hot zone.

Samples were quenched by releasing the specimen rapidly into a beaker of ice water or brine, situated no more than 10 mm from the exterior of the alumina working tube. The specimen was rapidly removed from the beaker and dried with compressed air to minimize the probability of dissolving the sample in water.

Thereafter, small pieces of the specimen were mounted in epoxy resin. The solidified mounted specimen was dry-polished on sandpaper; the grid sizes were 240, 400, 800, 1200 and 2000 P, respectively. Finally, the sample was polished on 3 and 1 micron diamond-coated surfaces. Overall, a well-polished cross-section of the sample was prepared using conventional dry metallographic grinding and polishing techniques. A dry technique was employed as a precaution because V_2O_5 has a solubility of 0.8 g/l in water [13]. For this reason, propylene glycol (Sigma Aldrich, Germany) and DP Lubricant Brown (Struers, Munich, Denmark) were used.

Before EPMA analysis, a sample was carbon-coated with a Leica EM SCD050 Coater (supplied by Leica Mikrosysteme GmbH, Vienna) in order to create a conductive surface. This avoids charge build-up of a specimen, which reduces thermal damaging of samples and improves the secondary electron signal, subsequently improving imaging. The samples for EPMA were analysed at 15 KV accelerating voltage and 40 nA beam current. All elements were measured on their Kα lines, using wavelength-dispersive spectrometers. Fe was calibrated on Fe_2O_3, Ti on TiO_2 and V on pure V, but the measured V mass fractions were adjusted as if V had been calibrated on vanadinite ($Pb_5(VO_4)_3Cl$). This was done to match the matrix of the calibration standard better with the (oxidic) matrix of the samples. The matrix correction in the probe software was based on the "X-PHI" model [14].

3.3. Application of the Phase Rule

The importance of the phase rule was discussed in our article on the Fe-V-O system in air [1]. The significance and value of the phase rule becomes more evident in the Fe-Ti-V-O system compared to lower order systems such as the Fe-V-O and Ti-V-O systems in air, owing to two or three solid phases that were in equilibrium with the slag phase for the investigated temperature range. For our system, the pressure is fixed at 1 atm (isobaric), hence the phase rule is expressed as follows:

$$f = c - p + 1. \tag{1}$$

In this case $c = 5$ (Fe, Ti, V , O_2 and N_2) and p = 3 or 4. If two solid phases (for example, rutile and ferropseudobrookite solid solutions) are in equilibrium with the slag and gas phase, $f = 2$. Therefore, two variables are at our discretion, and the remainder are fixed. Such a system is bivariant. The temperature is fixed at the desired temperature and oxygen partial pressure, an intensive property, is fixed at 0.21 atm, hence fully defining the system. If only one solid phase is in equilibrium with the slag phase, $f = 3$ (trivariant). With three variables at our discretion, the composition, another intensive property, of one specie in the slag or solid solution is fixed together with the temperature, which was fixed at the furnace set-point and oxygen partial pressure again fixed at 0.21 atm. However, fixing the composition of the slag or solid solution was not possible, given that the aim was to determine the compositions of both solutions experimentally. Knowing that the initial composition was at our discretion, it was possible to directly chose a set of initial compositions that was confined to an area where the slag was in equilibrium with one solid phase. This allowed one to vary the equilibrium slag and solid composition indirectly. In such a case, more than one experiment was done at the same temperature. In the described manner, the phase rule was applied successfully to unambiguously determine the thermodynamic state of the system.

4. Thermodynamic modelling

4.1. Stoichiometric Compounds

The Gibbs energies of stoichiometric compounds and of the components of solution phases are expressed in the form of $G_m - \sum H_{SER}$ and are also a function of temperature. The $\sum H_{SER}$ (standard element reference - SER) is the

sum of enthalpies of the elements at 298 K and 1 bar pressure. For thermodynamic assessment purposes, the standard molar Gibbs energy of stoichiometric compounds is reported by the combination of standard enthalpy of formation, standard entropy and heat capacity terms:

$$G^{\circ}(T) = \left(\Delta H_{f,298K} + \int_{298K}^{T} C_p(T)dT\right) - T\left(S^{\circ}_{298K} + \int_{298K}^{T} (C_p(T)/T)dT\right) \quad (2)$$

4.2. Gas Phase

The system pressure was kept constant at approximately 1 atm (absolute) for all experiments and modelling efforts, therefore a gas phase exhibits ideal behaviour. Such an assumption is validated by the following limiting condition [15]:

$$\lim_{P\to 0} \frac{f_i}{p_i} \equiv 1. \quad (3)$$

Equation 3 states that when pressure goes to zero, all gases behave ideally. As a result, the assumption of ideal behaviour at 1 atm (absolute) holds, and the molar Gibbs energy of the gas phase is given by Equation 4 [15]:

$$G_m = \sum_i x_i G_i^{\circ} + RT \sum_i x_i ln x_i + RT ln(P_i/P_{\circ}) \quad (4)$$

where x_i is the molar fraction of gas phase constituent i, $P_{\circ}$ is the standard pressure of 1 atm and P_i is the partial pressure.

4.3. Liquid Phase

The modified quasichemical model (MQM) [16, 17], which takes into account short-range ordering of second nearest neighbours (SNN), was used in our previous studies to describe the liquid phase in the Fe-V-O and Ti-V-O systems. Xie et al. [18] assumed that liquid V_2O_5 is made up of the building unit VO_4^{3-}, which in turn corresponds to VO^{3+} cation species. The same author stated that $V_2O_7^{4-}$ can also be used as a building unit. Hudon and Jung [19] and Rahman et al. [20] adopted $P_2O_7^{4-}$ as building unit of P_2O_5 in the $CaO-P_2O_5$ and $SiO_2-P_2O_5$ systems, respectively. This approach has also been adopted by FactSage for describing slag phases containing P_2O_5 [5]. In addition, it was found from the study of Kawakita et al. [21] that the characteristics of liquid P_2O_5 is similar to liquid V_2O_5. Therefore, to remain consistent with the modelling methods of our previous studies and that of the FToxid database in FactSage, V_2O_5 will have the building unit $V_2O_7^{4-}$, which can be surrounded by four broken oxygen atoms. This constitutes $V_2O_3^{4+}$ as corresponding cation species. The quasichemical reaction between cations in liquid Fe-Ti-V-O in air can be expressed as:

$$(Fe^{3+} - Fe^{3+}) + (V_2O_3^{4+} - V_2O_3^{4+}) = 2(Fe^{3+} - V_2O_3^{4+}) \qquad \Delta g_{Fe^{3+}-V_2O_3^{4+}} \quad (5)$$

$$(Fe^{2+} - Fe^{2+}) + (V_2O_3^{4+} - V_2O_3^{4+}) = 2(Fe^{2+} - V_2O_3^{4+}) \qquad \Delta g_{Fe^{2+}-V_2O_3^{4+}} \quad (6)$$

$$(Ti^{4+} - Ti^{4+}) + (V_2O_3^{4+} - V_2O_3^{4+}) = 2(Ti^{4+} - V_2O_3^{4+}) \qquad \Delta g_{Ti^{4+}-V_2O_3^{4+}} \quad (7)$$

$$(Ti^{3+} - Ti^{3+}) + (V_2O_3^{4+} - V_2O_3^{4+}) = 2(Ti^{3+} - V_2O_3^{4+}) \qquad \Delta g_{Ti^{3+}-V_2O_3^{4+}} \quad (8)$$

$$(Ti^{4+} - Ti^{4+}) + (Fe^{3+} - Fe^{3+}) = 2(Ti^{4+} - Fe^{3+}) \qquad \Delta g_{Ti^{4+}-Fe^{3+}} \quad (9)$$

$$(Ti^{4+} - Ti^{4+}) + (Fe^{2+} - Fe^{2+}) = 2(Ti^{4+} - Fe^{2+}) \qquad \Delta g_{Ti^{4+}-Fe^{2+}} \quad (10)$$

$$(Ti^{3+} - Ti^{3+}) + (Fe^{2+} - Fe^{2+}) = 2(Ti^{3+} - Fe^{2+}) \qquad \Delta g_{Ti^{3+}-Fe^{2+}} \quad (11)$$

$$(Fe^{3+} - Fe^{3+}) + (Ti^{3+} - Ti^{3+}) = 2(Fe^{3+} - Ti^{3+}) \qquad \Delta g_{Fe^{3+}-Ti^{3+}} \tag{12}$$

$$(Fe^{3+} - Fe^{3+}) + (Fe^{2+} - Fe^{2+}) = 2(Fe^{3+} - Fe^{2+}) \qquad \Delta g_{Fe^{3+}-Fe^{2+}} \tag{13}$$

$$(Ti^{4+} - Ti^{4+}) + (Ti^{3+} - Ti^{3+}) = 2(Ti^{4+} - Ti^{3+}) \qquad \Delta g_{Ti^{4+}-Ti^{3+}} \tag{14}$$

where $\Delta g_{Fe^{3+}-V_2O_3^{4+}}$, $\Delta g_{Fe^{2+}-V_2O_3^{4+}}$, $\Delta g_{Ti^{4+}-V_2O_3^{4+}}$, $\Delta g_{Ti^{3+}-V_2O_3^{4+}}$, $\Delta g_{Ti^{4+}-Fe^{3+}}$,$\Delta g_{Ti^{4+}-Fe^{2+}}$, $\Delta g_{Ti^{3+}-Fe^{3+}}$, $\Delta g_{Fe^{3+}-Fe^{2+}}$ and $\Delta g_{Ti^{4+}-Ti^{3+}}$ are non-configurational Gibbs energy changes for the formation of 2 moles of SNN pairs.

Optimized parameters for the binary FeO-Fe_2O_3 slag solution are taken from Degterov et al. [22]. The quasi-chemical model parameters of the $TiO_2-Ti_2O_3$ system were first optimized by Erikson and Pelton [3] and later again by Kang et al. [23] in response to the publication of more recent experimental data. Hence, the parameters of Kang et al. [23] are used in this study. The optimized parameters for the binary V_2O_5-Fe_2O_3, V_2O_5-FeO, V_2O_5-TiO_2 and V_2O_5-Ti_2O_3 slag solutions were taken from Malan et al. [1, 2].

The Fe-Ti-O system was thermodynamically assessed by Erikson and Pelton [3] and later again by Erikson et al. [4]. The optimized quasichemical parameters from their studies are used in the thermodynamic assessment of this study. However, all the assessments of the Fe-Ti-O system were performed under reducing conditions. Therefore, it was undertaken to partially optimize the Fe-Ti-O system under oxidizing conditions with experimental data from this study. This required optimizing parameters related to the $Fe_2O_3-TiO_2$ solution and back-calculating the Fe-Ti-O phase diagram in air. The molar Gibbs energy of the $Fe_2O_3-TiO_2$ solution is expanded as follows:

$$G_m = n_{TiO_2} g^{\circ}_{TiO_2} + n_{Fe_2O_3} g^{\circ}_{Fe_2O_3} - T\Delta S^{config} + n_{Ti^{4+}-Fe^{3+}}(\Delta g_{Ti^{4+}-Fe^{3+}}/2). \tag{15}$$

where $\Delta g_{Fe^{3+}-Ti^{4+}}$ can be expanded as an empirical polynomial function in the mole fractions of pairs.

$$\Delta g_{Fe^{3+}-Ti^{4+}} = \Delta g^{\circ}_{Fe^{3+}-Ti^{4+}} + \sum_{i\geq 1} g^{i0}_{Fe^{3+}-Ti^{4+}} X^{i}_{Fe^{3+}-Fe^{3+}} + \sum_{j\geq 1} g^{0j}_{Fe^{3+}-Ti^{4+}} X^{j}_{Ti^{4+}-Ti^{4+}} \tag{16}$$

$\Delta g^{\circ}_{Fe^{3+}-Ti^{4+}}$, $g^{0j}_{Ti^{4+}-Fe^{3+}}$, and $g^{i0}_{Fe^{3+}-Ti^{4+}}$ are all temperature-dependent adjustable model parameters, and were optimized to reproduce the liquidus within the limits of experimental error. Furthermore, it was estimated with FactSage that Fe_2TiO_5 (if selected from the list of pure compounds) melts congruently in the Fe-Ti-O system in air. The existence of stable solid phase at the composition of Fe_2TiO_5 can be an indication of short range ordering in the liquid phase at the same composition. This is because $\Delta g^{\circ}_{Fe^{3+}-Ti^{4+}}$ becomes significant at composition of maximum short range ordering. It was shown by Xie et al. [18], Hudon and Jung [19], Wang [24], Prostakova et al. [25] that maximum short range ordering usually occurs at the intermediate compound with the highest melting point (congruent melting) and the minimum mixing enthalpy.

A Kohler interpolation method, which is symmetric in nature, is used as an initial approach for estimating thermodynamic properties and phase diagram data from binary model parameters. This interpolation method is based on the assumption that all components are chemically similar and has been successful in describing the slag phases of higher order systems [26, 27, 28, 25, 1, 2].

4.4. Modelling Solid Solutions

Solid solutions in the Fe-Ti-V-O system in air were developed within the framework of the compound energy formalism (CEF) [29, 30, 31]. This means that a mathematical expression such as the CEF is more general than the actual physical model and can be applied to various constituents with different behaviour in a phase. When such a generalised expression is obtained, it is referred to as a formalism. It has been shown that the CEF is well suited to model solid solutions with two or more distinct sub-lattices. Furthermore, it allows for cations and anions of different valances to mix in different sub-lattices, corresponding to the structure of a solid solution [8].

$$G_m = \sum_i \sum_j X_i X_j G_{ij} - TS_{config} + G_E \tag{17}$$

X_i and X_j in Equation 17 represent the site fractions of constituents i and j on the first and second sublattices, respectively. G_E is the excess Gibbs energy and S_{config} is the configurational entropy, and is given by Equation 18:

$$S_{config} = -R(a\sum_i X_i LnX_i + b\sum_j X_j LnX_j) \tag{18}$$

with a and b being the stoichiometric constants of each lattice and R the ideal gas constant.

4.4.1. Hematite Solid Solution

The model for the hematite solid solution was developed to account for V_2O_5 and TiO_2 dissolution in the hematite phase. The hematite solid solution is expanded from our study on the Fe-V-O system in air to also account for the dissolution of TiO_2 and has the chemical formula, $(Fe^{3+}, Ti^{4+}, V^{5+}, Va)_2(O^{2-})_3$. Therefore, the molar Gibbs energy of the hematite solid solution is given by Equation 19:

$$\begin{aligned} G_{hem} = {} & X_{Fe^{3+}}X_{O^{2-}}G^{\circ}_{Fe^{3+}:O^{2-}} + X_{V^{5+}}X_{O^{2-}}G^{\circ}_{V^{5+}:O^{2-}} + X_{Ti^{4+}}X_{O^{2-}}G^{\circ}_{Ti^{4+}:O^{2-}} + X_{Va}X_{O^{2-}}G^{\circ}_{Va:O^{2-}} + \\ & + 2RT(X_{Fe^{3+}}lnX_{Fe^{3+}} + X_{V^{5+}}lnX_{V^{5+}} + X_{Ti^{4+}}lnX_{Ti^{4+}} + X_{Va}lnX_{Va}) + 3RT(X_{O^{2-}}lnX_{O^{2-}}) + \\ & G_E \end{aligned} \tag{19}$$

where $G_E = 0$.

Expressions for end-member components related to the dissolution of V_2O_5, were derived in our previous study [1]. A schematic of the hematite solid solution with a neutral triangle and end-member components is shown in Figure 1.

Four end-member species are presented on the corners of the square, of which three compounds have a net charge higher or lower than zero. Expressions for end-member components related to the dissolution of V_2O_5, were derived in our previous study. These are the end-members $G^{\circ}_{V^{5+}:O^{2-}Hem}$ and $G^{\circ}_{Va:O^{2-}Hem}$. The neutral compound, $G^{\circ}_{(3/4Ti,1/4Va)_2:O_3}$ has a hematite-related structure and is a combination of $G^{\circ}_{Va_2:O_3}$ and $G^{\circ}_{Ti_2:O_3}$.

$$6/4G^{\circ}_{TiO2(s)-Hem} = \frac{3}{4}G^{\circ}_{Ti^{4+}:O^{2-}} + \frac{1}{4}G^{\circ}_{Va:O^{2-}} + 2RT\left(\frac{3}{4}ln\frac{3}{4} + \frac{1}{4}ln\frac{1}{4}\right) \tag{20}$$

The third term in Equation 20 is an entropy of mixing attribution on the anion and cation lattices. The term, $G^{\circ}_{TiO2(s)-Hem}$ was optimised with respect to its enthalpy of formation and standard entropy.

4.4.2. Rutile Solid Solution

The experimental data from [32] indicated a solubility region of Fe_2O_3(s) in rutile. The Gibbs energy of the solution is developed within the framework of the CEF (Equation 17) and expanded from our study on the Ti-V-O system in air. Similar, to modelling of V_2O_5 and TiO_2 dissolution in the hematite phase, it is assumed in the rutile solid solution model that all cations mix in one lattice and all anions in a second lattice. That said, V and Fe dissolve substitutionally in the rutile phase and vacancies are formed on both cation and anion sub-lattices to account for charge neutrality, and has the chemical formula, $(Ti^{4+}, Fe^{3+}, V^{5+}, Va)(O^{2-}, Va)_2$. Moreover, the rutile solid solution model from our work on the Ti-V-O system in air [2] is expanded and eight end-member species are formed (see Figure 2) from which expressions were already derived for three end-members. The molar Gibbs energy of the rutile solid solution to model dissolution of V_2O_5 and Fe_2O_3(s) is expressed as follows:

$$\begin{aligned} G_{Rut} = {} & X_{Ti^{4+}}X_{O^{2-}}G^{\circ}_{Ti^{4+}:O^{2-}} + X_{Ti^{4+}}X_{Va}G^{\circ}_{Ti^{4+}:Va} + X_{V^{5+}}X_{O^{2-}}G^{\circ}_{V^{5+}:O^{2-}} + X_{V^{5+}}X_{Va}G^{\circ}_{V^{5+}:Va} + \\ & X_{Va}X_{O^{2-}}G^{\circ}_{Va:O^{2-}} + X_{Fe^{3+}}X_{O^{2-}}G^{\circ}_{Fe^{3+}:O^{2-}} + X_{Fe^{3+}}X_{Va}G^{\circ}_{Fe^{3+}:Va} + X_{Va}X_{Va}G^{\circ}_{Va:Va} + \\ & RT(X_{Ti^{4+}}lnX_{Ti^{4+}} + X_{V^{5+}}lnX_{V^{5+}} + X_{Va}lnX_{Va} + X_{Fe^{3+}}lnX_{Fe^{3+}}) + 2RT(X_{O^{2-}}lnX_{O^{2-}} + X_{Va}lnX_{Va}) + \\ & G_E \end{aligned} \tag{21}$$

where $G_E = 0$.

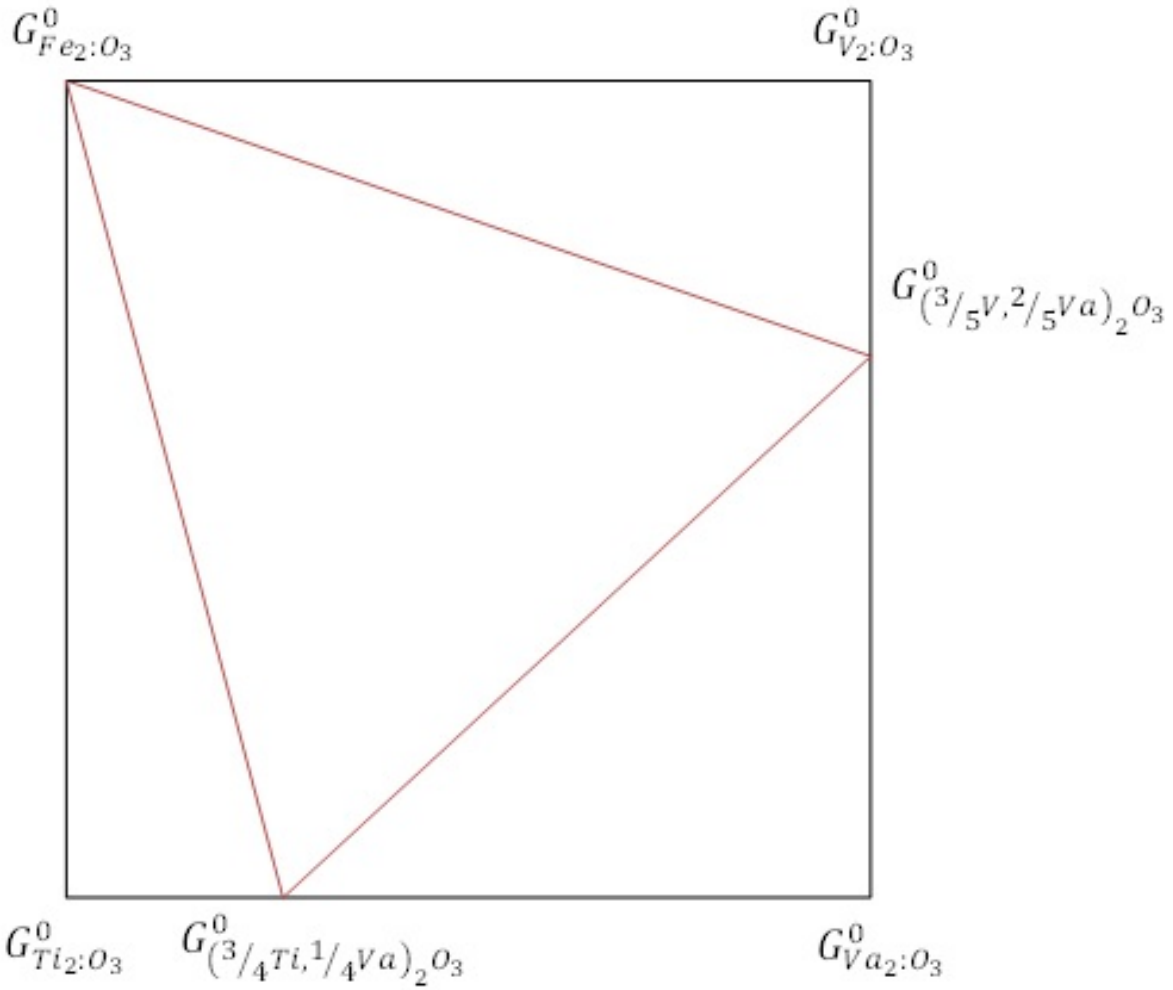

Figure 1: The neutral triangle (in red) in the expanded hematite solid solution. Each corner represents an end-member of the solution.

To include Fe_2O_3(s) in the rutile solid solution, four end-member species related to the Fe-Ti-O system are presented on the back corners of the cube. The neutral end-member, $G^{\circ}_{Ti^{4+}:O^{2-}}$ corresponds to stoichiometric rutile, while the other three compounds have a net charge of higher or lower than zero and cannot physically exist. The neutral compound, $G^{\circ}_{(Fe)(3/4O,1/4Va)_2}$ has a rutile-related structure and is a combination of $(Fe^{3+})(O^{2-})$ and $(Fe^{3+})(Va)$. The thermodynamic properties of $FeO_{1.5}$ are derived in a similar way to the γ modification of the oxide $TiO_{1.5}$ from the study of Cancarevic et al. [33].

$$G^{\circ}_{FeO_{1.5}} = 1/2G^{\circ}_{Fe_2O_3-Rut} = \frac{3}{4}G^{\circ}_{Fe^{3+}:O^{2-}} + \frac{1}{4}G^{\circ}_{Fe^{3+}:Va} + 2RT\left(\frac{3}{4}ln\frac{3}{4} + \frac{1}{4}ln\frac{1}{4}\right) \tag{22}$$

The additional end-members from the rutile solid solution are derived and expressed as follows:

$$G^{\circ}_{Ti^{4+}:Va} = G^{\circ}_{TiO_2} - G^{\circ}_{O_2(g)} \tag{23}$$

$$G^{\circ}_{Ti^{4+}:O^{2-}} - G^{\circ}_{Fe^{3+}:Va} = G^{\circ}_{Ti^{4+}:Va} - G^{\circ}_{Fe^{3+}:O^{2-}}. \tag{24}$$

Equation 22, Equation 23 and Equation 24 are combined and rearranged to obtain expressions for $G^{\circ}_{Fe^{3+}:Va}$ and $G^{\circ}_{Fe^{3+}:O^{2-}}$:

$$G^{\circ}_{Fe^{3+}:Va_2} = -\frac{3}{4}G^{\circ}_{O_{2(g)}} + \frac{1}{2}G^{\circ}_{Fe_2O_3-Rut} + 2RT\left(\frac{3}{4}ln\frac{3}{4} + \frac{1}{4}ln\frac{1}{4}\right) \tag{25}$$

$$G^{\circ}_{Fe^{3+}:O_2^{2-}} = \frac{1}{4}G^{\circ}_{O_{2(g)}} + \frac{1}{2}G^{\circ}_{Fe_2O_3-Rut} + 2RT\left(\frac{3}{4}ln\frac{3}{4} + \frac{1}{4}ln\frac{1}{4}\right). \tag{26}$$

Two new end-members, marked, $G^{\circ}_{Va:Va_2}$ and $G^{\circ}_{V^{5+}:Va_2}$, and one neural apex on the line $G^{\circ}_{V^{5+}:O_2^{2-}}$, $G^{\circ}_{Fe^{3+}:O_2^{2-}}$ marked $G^{\circ}_{(\frac{1}{2}V^{5+},\frac{1}{2}Fe^{3+}):O_2^{2-}}$ are observed in Figure 2, and Gibbs energy expressions can be derived from reciprocal relations:

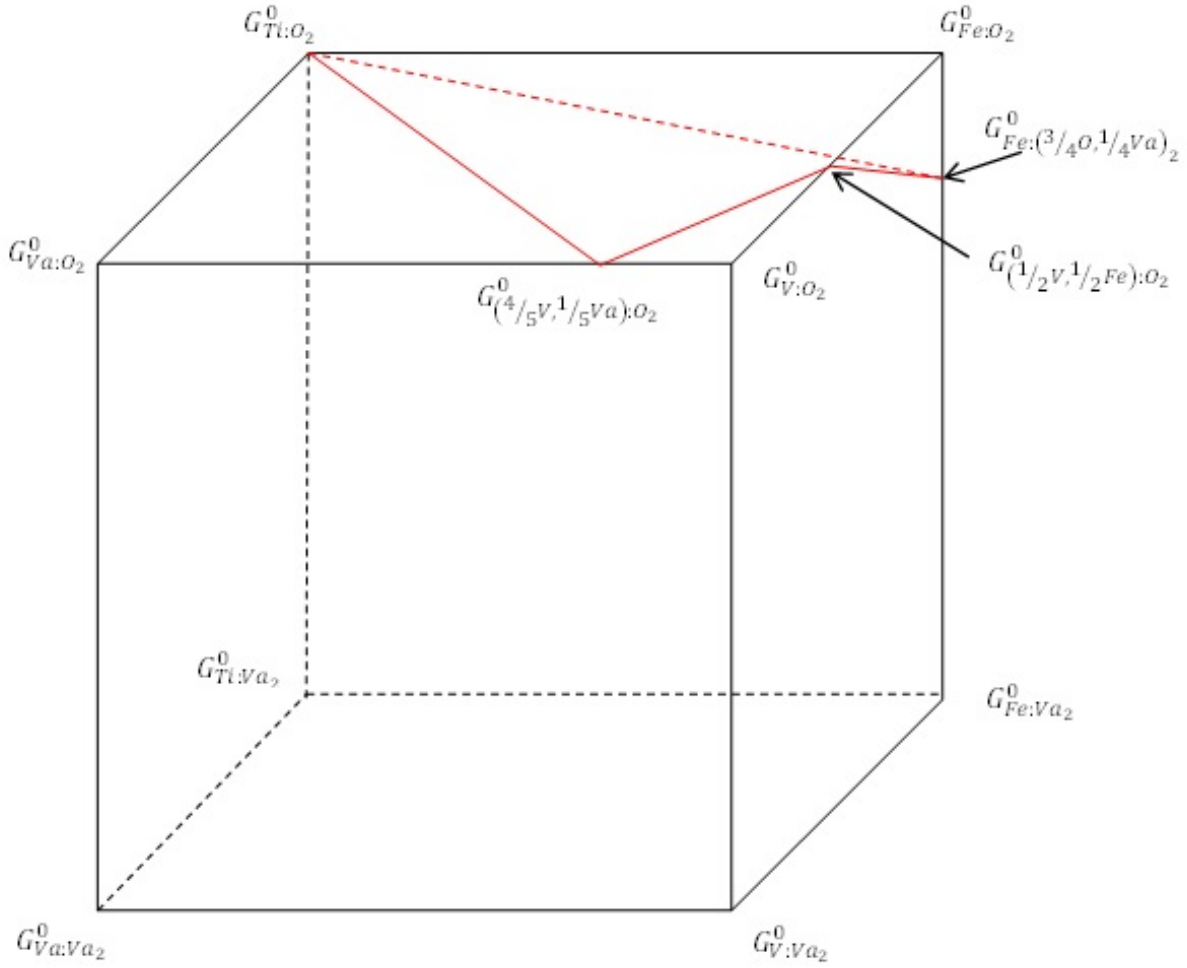

Figure 2: The neutral plane (in red) in the expanded rutile solid solution. Each corner represents an end-member of the solution.

$$G^{\circ}_{V^{5+}:O_2^{2-}} + G^{\circ}_{Fe^{3+}:Va_2} = G^{\circ}_{V^{5+}:Va_2} + G^{\circ}_{Fe^{3+}:O_2^{2-}} \tag{27}$$

$$G^{\circ}_{Ti^{4+}:O_2^{2-}} + G^{\circ}_{Va:Va_2} = G^{\circ}_{Ti^{4+}:Va_2} + G^{\circ}_{Va:O_2^{2-}}. \tag{28}$$

The two new end-members from exchange reactions 27 and 28 are derived by substituting for known expressions from Equation 23-Equation 26, and Equation 21 - 23 in Malan et al. [2], followed by rearrangement:

$$G^{\circ}_{Va:Va_2} = -G^{\circ}_{O_{2(g)}} \tag{29}$$

$$G^{\circ}_{V^{5+}:Va_2} = \frac{1}{2}G^{\circ}_{V_2O_5(s)-Rut} - G^{\circ}_{O_2(g)} - \frac{5}{2}RT\left(\frac{4}{5}ln\frac{4}{5} + \frac{1}{5}ln\frac{1}{5}\right). \quad (30)$$

4.4.3. Ferropseudobrookite Solid Solution

It is mentioned in section 2 that the dissolution of TiO_2(s) and Fe_2O_3(s) in ferropseudobrookite solid solution under oxidizing conditions cannot be reproduced with the available model in FactSage. Nevertheless, a small solubility of V_2O_5 in the Fe_2TiO_5(s) phase was observed from the experimental results of this study (see section 6).

To include solubility of V_2O_5 in the existing model of ferropseudobrookite solid solution would require expanding the solution to include Fe^{3+}, Ti^{4+} and V^{5+} ions. The number of end-members will increase significantly, provided Fe^{3+}, Ti^{4+} and V^{5+} ions are included in both sub-lattices. However, there is no experimental evidence to support this ion distribution configuration. Moreover, the new end-members need to be mathematically derived, from which end-members consisting of Fe^{3+}, Ti^{4+} and V^{5+} ions require optimization from experimental data. The only solubility data of ferropseudobrookite solid solution under oxidizing conditions are available from this study, ranging from 1000 °C to 1400 °C.

It was not possible to model ferropseudobrookite solid solution under oxidizing conditions with the CEF owing to the shortage of occupancy data. In other words, the distribution of Fe^{3+}, Ti^{4+} and V^{5+} ions between the sub-lattices are not known. Nevertheless, the Gibbs energy of ferropseudobrookite solid solution is represented by a simple polynomial model. The components of the solution are Fe_2TiO_5(s) and V_2O_5(s).

$$G_m = x_{V_2O_5}G^{\circ}_{V_2O_5} + x_{Fe_2TiO_5}G^{\circ}_{Fe_2TiO_5} + RT\left(x_{V_2O_5}Lnx_{V_2O_5} + x_{Fe_2TiO_5}Lnx_{Fe_2TiO_5}\right) + G_E \quad (31)$$

and the excess molar Gibbs energy of Equation 31 is given by Equation 32:

$$G_E = \sum_i \sum_j x_i x_j L^{qp}_{ij}, \quad (32)$$

L^{qp}_{ij} are interaction parameters that may be temperature-dependent. The powers of q and p are ≥ 0 and < 2. The interaction parameters are optimised from experimental data to reproduce ferropseudobrookite solid solution accurately.

Although this model is a simplification and does not accurately represent the bonding between constituents of the ferropseudobrookite solid solution and their configuration, it still has the ability to reproduce the measured composition of ferropseudobrookite solid solution to some extent. Furthermore, with the inclusion of the ferropseudobrookite solid solution, slag, rutile and hematite solid solutions compositions were more accurately reproduced. If the ferropseudobrookite solid solution had been modelled only as Fe_2TiO_5(s), the composition of Fe, Ti and V in the slag phase would have been more inaccurate.

5. Sequence of Optimization

The principle of data fitting and parameter optimisation is based on a least-squares method. That is, an objective function is expressed as the difference between the calculated value of a given property and an experimental value of the same property. This difference is known as the residual. It is possible to acquire a set of optimised model parameters by minimizing the sum of the square of the residual over all measured points. The optimisation was performed using the OPTIGAGE tool in FactSage 7.0 which has the ability to consider all types of data simultaneously. The guidelines set by Lukas et al. [8] were closely followed in this assessment.

In the first step of the optimisation, $G^{\circ}_{V_2O_5(s)-Rut}$ from our study on the Ti-V-O system in air was re-optimised by considering the experimental data from that study. This is because of two additional end-members, ($G^{\circ}_{V^{5+}:Va_2}$ and $G^{\circ}_{Va:Va_2}$) that were derived in subsubsection 4.4.2. Thereafter, the quasichemical model parameters related only to the Fe-Ti-O system, and enthalpy of formations and standard entropies of $G^{\circ}_{TiO_2(s)-hem}$ and $G^{\circ}_{Fe_2O_3-Rut}$ from solid solutions, hematite and rutile, were optimised. At the same time, thermodynamic properties of Fe_2TiO_5 and parameters of the ferropseudobrookite solid solution were optimised. In these steps, parameters from different solutions were optimised independently. All thermodynamic parameters were simultaneously optimised in the final step of optimisation by considering all experimental data from this study.

6. Results

6.1. Phase Characterisation and Quantification

Polished and coated samples were analysed with EPMA and SEM-EDS; however only results from EPMA are shown in Table 2. Before experiments were carried out, a set of isothermal planes (not shown here) was calculated from optimised binary parameters of the Fe-Ti-O, Fe-V-O and Ti-V-O systems in air to estimate a range of plausible starting compositions for experiments on the Fe-Ti-V-O system in equilibrium with air. Therefore, the initial compositions shown in Table 2 were estimated meticulously to have one or two solid phases in equilibrium with the slag phase, and to have sufficient amount of each phase for SEM-EDS analysis and EPMA.

To confirm sample homogeneity, at least ten points of each phase were analysed to calculate a set of standard deviations for each element. For samples at and above 1200 °C, at least 15 areas of the slag phase were analysed owing to the occurrence of precipitates. Oxygen concentration was calculated on the basis of stoichiometry (St.) by assuming V is in the 5+, Fe in the 3+ and Ti in the 4+ oxidation state. The standard deviation (σ) of each element is shown in the table next to its mean concentration. The results from EPMA en SEM-EDS compared relatively well, but small differences are observed owing to the overlapping of X-ray emission peaks of V and Ti. Therefore, only EPMA results were normalised and used in the thermodynamic assessment of the Fe-Ti-V-O system in air.

Table 2: Summary of raw data from the Fe-Ti-V-O system in air analysed using EPMA.

Experiment	Initial composition wt.%			Temperature °C	Phases at equilibrium	Final composition in wt.%							
	V2O5	Fe2O3	TiO2			Fe	Fe (STD)	V	V (STD)	Ti	Ti (STD)	O (Stoichiometry)	Total
1	60	10	30	1000	Slag	10.28	0.64	47.14	0.94	2.26	0.42	42.94	102.63
					Rutile	4.54	0.10	10.84	0.07	46.39	0.14	41.47	103.23
2	33	33	33	1000	Slag	11.98	0.61	42.88	0.17	2.30	0.13	40.36	97.52
					Rutile	5.25	0.14	11.07	0.12	45.20	0.23	41.17	102.68
					Ferropseudobrookite	45.51	0.26	4.01	0.35	18.13	0.24	34.83	102.47
3	20	70	10	1000	Slag	12.95	1.25	46.70	1.16	0.55	0.14	42.61	102.81
					Hematite	67.07	0.94	1.77	0.14	1.31	0.08	31.09	101.24
					Ferropseudobrookite	45.97	0.79	7.03	0.59	13.04	0.79	33.99	100.02
4	70	15	15	1000	Slag	11.46	0.31	46.40	0.29	2.63	0.11	43.11	103.60
					Rutile	4.89	0.09	11.15	0.18	45.40	0.37	41.21	102.64
5	60	10	30	1100	Slag	14.43	1.46	44.42	0.89	2.70	0.31	42.89	104.43
					Rutile	4.26	0.13	11.06	0.09	45.74	0.10	41.09	102.15
6	50	12	38	1100	Slag	12.54	1.39	45.73	1.42	2.52	0.50	42.98	103.78
					Rutile	4.22	0.06	11.58	0.19	44.85	0.34	40.89	101.54
7	20	70	10	1100	Slag	17.01	0.94	41.89	0.74	0.94	0.16	40.83	100.68
					Hematite	66.78	0.17	1.84	0.04	1.84	0.07	31.37	101.83
					Ferropseudobrookite	46.77	0.29	6.87	0.09	13.69	0.14	34.64	101.97
8	33	33	33	1100	Slag	13.56	0.85	42.40	0.73	3.51	0.26	41.46	100.93
					Rutile	4.49	0.10	10.80	0.12	45.53	0.28	40.85	101.66
					Ferropseudobrookite	44.00	0.43	3.75	0.16	18.72	0.37	34.36	100.83
9	33	33	33	1200	Slag	16.11	0.70	41.31	0.69	3.90	0.56	41.97	103.29
					Rutile	3.87	0.08	10.09	0.06	47.78	0.12	41.53	103.27
					Ferropseudobrookite	43.78	0.19	4.18	0.10	19.64	0.08	35.23	102.84
10	60	20	20	1200	Slag	17.20	1.92	41.17	1.47	3.67	0.38	42.17	104.20
					Rutile	3.51	0.13	10.55	0.10	46.67	0.20	40.99	101.70
11	50	20	30	1200	Slag	18.00	1.46	39.91	0.61	4.22	0.73	41.90	104.03
					Rutile	3.55	0.13	10.35	0.13	47.31	0.08	41.27	102.47
12	20	70	10	1200	Slag	20.17	0.72	40.08	0.91	0.78	0.16	40.66	101.68
					Hematite	62.20	0.97	2.91	0.38	2.70	0.10	30.82	98.63
					Ferropseudobrookite	44.78	1.52	7.33	0.36	13.06	0.92	33.73	98.89
13	40	20	40	1300	Slag	20.63	1.66	37.39	1.89	5.01	1.37	41.58	104.20
					Rutile	3.02	0.11	8.27	0.10	49.74	0.14	41.04	101.70
14	20	65	15	1300	Slag	30.86	1.59	29.82	1.28	2.49	0.47	38.34	101.51
					Hematite	61.99	0.16	2.75	0.09	4.28	0.12	31.66	100.68
					Ferropseudobrookite	44.45	0.28	5.65	0.24	15.81	0.22	34.10	100.00
15	50	10	40	1300	Slag	18.13	1.26	40.59	1.52	2.75	0.78	41.50	102.98
					Rutile	2.57	0.11	9.63	0.27	48.30	0.37	40.95	101.44
16	20	30	50	1300	Slag	20.87	1.62	33.85	1.09	7.34	0.63	40.46	102.52
					Rutile	3.05	0.16	8.27	0.19	49.65	0.09	40.99	101.96
					Ferropseudobrookite	41.26	0.17	3.84	0.07	21.55	0.09	35.16	101.81
17	40	20	40	1400	Slag	22.70	2.44	32.21	2.72	8.56	1.12	40.77	104.24
					Rutile	2.08	0.03	7.61	0.05	50.65	0.09	40.73	101.06
18	20	20	60	1400	Slag	27.92	2.03	22.54	2.57	13.15	1.98	38.49	102.10
					Rutile	2.48	0.14	6.00	0.20	51.81	0.54	40.41	100.70
19	15	75	10	1400	Slag	31.10	0.70	27.27	1.00	5.90	0.71	38.72	102.99
					Hematite	59.48	0.86	2.76	0.18	6.56	0.20	32.12	100.92

All analysed samples from 1000 °C to 1300 °C have two or three homogeneous condensed phases in equilibrium with air. All analysed samples at 1400 °C have only two phases in equilibrium with air owing to ferropseudobrookite (Fe_2TiO_5(s)) melting congruently at 1388 °C. However, this congruent melting point was estimated with FactSage and has not been determined experimentally. Results from the experiments indicate that the congruent melting point of ferropseudobrookite solid solution is between 1300 °C and 1400 °C. The measured molar ratio of Fe to Ti in ferropseudobrookite solid solution is higher when in equilibrium with the slag and hematite solid solution compared to a sample where ferropseudobrookite solid solution is in equilbirium with the slag and rutile solid solution. The

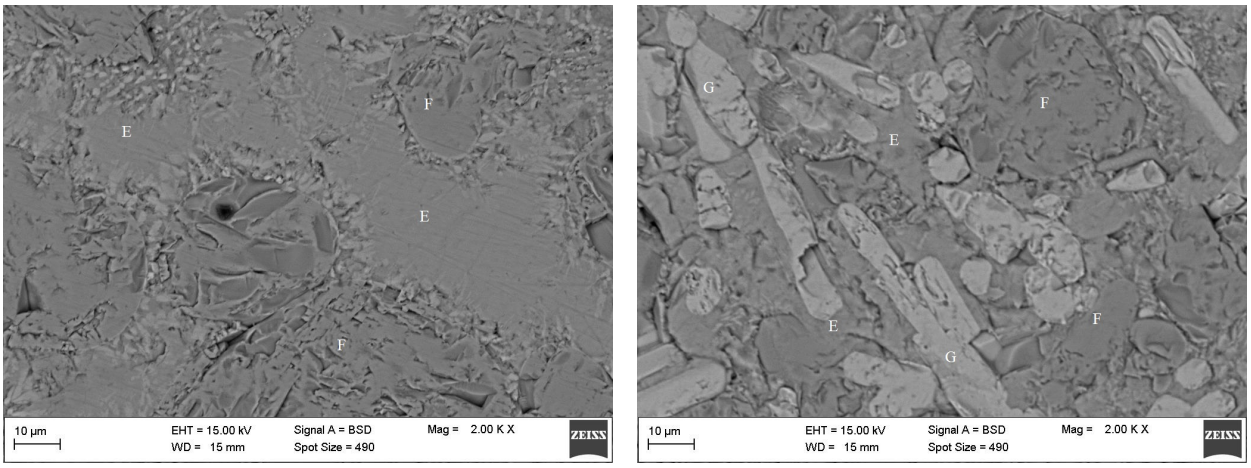

(a) Two phases.

(b) Three phases.

Figure 3: BSE micrographs of quenched samples at 1000 °C: light crystals in (a) and (b) are rutile solid solution (F) and the non-crystalline dark glassy phase is molten slag (E). The darker crystals in (b) are ferropseudobrookite solid solution (G).

measured molar ratio of Fe to Ti in the ferropseudobrookite solid solution of the latter constitutes that of Fe_2TiO_5(s). Furthermore, a small amount of V_2O_5 has dissolved in ferropseudobrookite.

It is also noted that a small amount of TiO_2 and V_2O_5 had dissolved in the hematite phase. Similarly, it is noted that a small amount of Fe_2O_3 and V_2O_5 had dissolved in the rutile phase. The dissolution of V_2O_5 in the hematite and rutile phases was already observed in experimental investigations of the Fe-V-O and Ti-V-O systems in air [1, 2].

Micrographs captured from the SEM back-scattered detector of samples quenched at 1000 °C, 1200 °C and 1400 °C are shown in Figure 3, Figure 4 and Figure 5. For the samples quenched at 1200 °C and 1400 °C, an appreciable amount of precipitation is observed in the molten slag phase and this is enhanced by an increase in Fe content. The samples at and above 1200 °C were analysed by following the analytical procedure outlined in our study on the Fe-V-O system in air [1]. The calculated standard deviations of samples quenched at 1400 °C were in some cases above 1 wt.%. Nevertheless, given the scarcity of data in this system, experimental data had to be accepted and used for the assessment.

6.2. Thermodynamic Calculations

Based on all experimental data from subsection 6.1, the optimised model and thermodynamic parameters for all phases in the Fe-Ti-V-O system in air are presented in Table 3 and Table 4. Using these parameters, phase equilibria and invariant properties are calculated and can be compared with literature data when these become available.

Isothermal sections at 1000 °C, 1100 °C, 1200 °C, 1300 °C and 1400 °C, calculated from optimised parameters, are shown in Figure 6, Figure 7, Figure 8, Figure 9, and Figure 10. All superimposed experimental data on the isothermal sections were considered during optimisation. The calculated liquidus projection along with primary fields and phases of the Fe-Ti-V-O system are shown in Figure 11. The calculated invariant reactions are shown in Table 5. No other phase diagram data were found in literature, consequently only experimental data from this study were used for the assessment.

Given that no previous study had thermodynamically evaluated the Fe-Ti-O system under oxidising conditions, it was undertaken to optimise quasichemical parameters only related to the Fe-Ti-O system. In this case, only one parameter was required to reproduce the liquidus accurately. $\Delta g^{\circ}_{Fe^{3+}-Ti^{4+}}$ has a major influence at compositions of maximum short-range ordering and in this case, maximum short-range ordering occurs at the congruent melting point of the ferropseudobrookite solid solution. Furthermore, no ternary parameters were required for the liquid phase.

Parameters of the rutile and hematite solid solutions were optimised to reproduce Fe_2O_3(s) and TiO_2(s) solubility. Moreover, a small adjustment was made to $G_{V_2O_5(s)-Rut}$ to reproduce solidus data from the Ti-V-O system in air, given that two additional end-members, ($G^{\circ}_{V^{5+}:Va_2}$ and $G^{\circ}_{Va:Va_2}$) were derived and optimised for the expanded model of rutile solid solution.

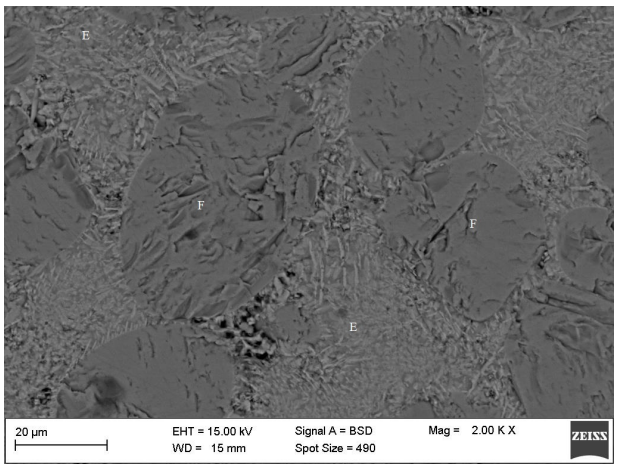

(a) Two phases.

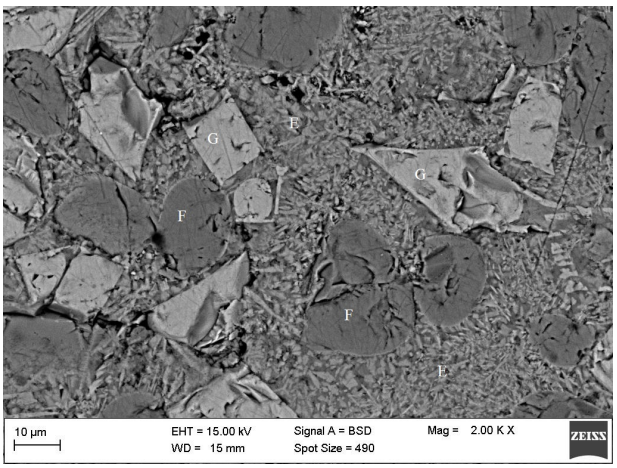

(b) Three phases.

Figure 4: BSE micrographs of quenched samples at 1200 °C: light crystals in (a) and (b) are rutile solid solution (F) and the non-crystalline dark glassy phase is molten slag (E). The darker crystals in (b) are ferropseudobrookite solid solution (G).

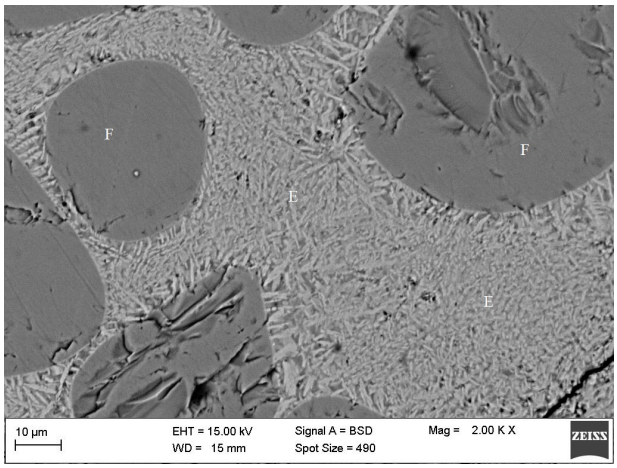

(a) Slag and rutile solid solution.

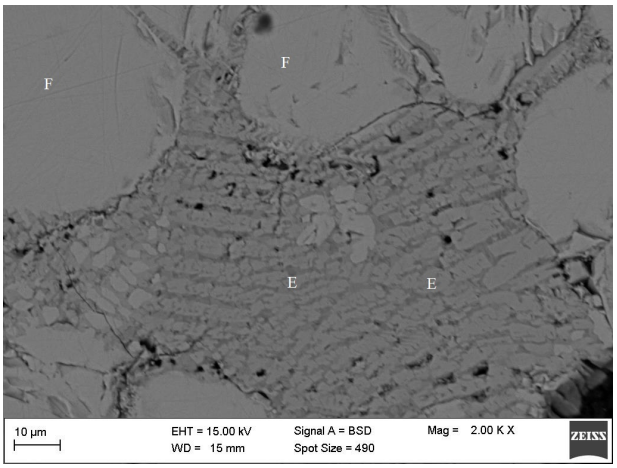

(b) Slag and hematite solid solution.

Figure 5: BSE micrographs of quenched samples at 1400 °C: light crystals in (a) are rutile solid solution (F) and darker crystals in (b) are hematite solid solution. The non-crystalline dark glassy phase in (a) and (b) is molten slag (E).

Table 3: The optimised parameters of solutions in the Fe-Ti-V-O system in air.

Liquid: FeO-Fe_2O_3-TiO_2-Ti_2O_3-V_2O_5

Quasichemical Model
FeO-Fe_2O_3 binary parameters
Taken from the study of Degterov et al. [22]
TiO_2-Ti_2O_3 binary parameters
Taken from the study of Kang et al. [23]
Ti_xO_x-FeO binary parameters
Taken from the study of Erikson et al. [4]
TiO_2-Fe_2O_3 binary parameters
$\Delta g^{\circ}_{Fe^{3+}-Ti^{4+}} = 152411 - 92.6727 * T$
TiO_2-Ti_2O_3 binary parameters
Taken from the study of Kang et al. [23]
V_2O_5-Fe_2O_3 binary parameters
Taken from Malan et al. [1]
V_2O_5-TiO_2 binary parameters
Taken from Malan et al. [2]

Hematite solid solution: $Fe_2O_3-TiO_2-V_2O_5$

$G^{\circ}_{TiO_2(s)-Hem} = G^{\circ}_{TiO_2(s)} - 12200.36 - 37.9927T - 12.4673T$ from 298 - 1673 K

$G^{\circ}_{V_2O_5(s)-Hem}$ - Taken from Malan et al. [1]

Rutile solid solution: $TiO_2-Fe_2O_3-V_2O_5$

$G^{\circ}_{Fe^{3+}:Va} = -\frac{3}{4}G^{\circ}_{O_{2(g)}} + \frac{1}{2}G^{\circ}_{Fe_2O_3(s)} + 71146.2 + 36.1442T + 9.35051T$ from 298 - 1673 K

$G^{\circ}_{Fe^{3+}:O^{2-}} = \frac{1}{4}G^{\circ}_{O_{2(g)}} + \frac{1}{2}G^{\circ}_{Fe_2O_3(s)} + 71146.2 + 36.1442T + 9.35051T$ from 298 - 1673 K

$G^{\circ}_{V_2O_5(s)-Rut} = G^{\circ}_{V_2O_5(s)} + 171607 - 32.96704T$

$G^{\circ}_{V^{5+}:Va_2} = \frac{1}{2}G^{\circ}_{V_2O_5(s)-Rut} - G^{\circ}_{O_2(g)} - 10.4009T$

$G^{\circ}_{Va:Va_2} = -G^{\circ}_{O_2(g)}$

Ferricpseudobrooktie solid solution: $Fe_2TiO_5-V_2O_5$

$L^{10}_{V_2O_5-Fe_2TiO_5} = 72366.5 - 62.3082T$

Table 4: The calculated enthalpies and entropies of pure compounds in the Fe-Ti-V-O.

Compound	$\Delta H^{\circ}_{f,298K}$	S°_{298K}	a	b	c	d	e	f	C_p range K	Reference
Solids										
Fe_2O_3(s)*	-825787.0	87.7285	137.01				-29.07640		298-2500	[5]
$FeVO_4$(s)	-1184723	128.436	129.51	24.71			-21.60000		298 - 973	[1]
$Fe_2V_4O_{13}$(s)	-3937787	382.628	388.83	73.83			-65.06000		298 - 973	[1]
Fe_2TiO_5(s)	-1744367	170.308	22.008				-31.00344		298-1673	This study
TiO_2(s)	-944750.0	50.460	77.848				- 33.67841	40.2940672	298- 2130	[5]
V_2O_5(s)	-1550590	130.559	25.970	50.00	5853.80	-76.76761	-7.541627		298- 943	[5]
Liquid										
Fe_2O_3(l)	-745158.3	139.467	137.01				-29.07640		298 - 2500	[1]
FeO(l)	-234643.2	78.4655	-18.024	31.00	1500.90		-25.33300		298 - 1644	[5]
			68.199						1644 - 2000	[5]
TiO_2(l)	-898726.0	72.068	77.840				- 33.67841	40.2940672	298- 2130	[5]
Ti_2O_3(l)	-1414375	130.17	169.96		-750.22		16.09649	-15.6552100	298 - 2115	[5]
V_2O_5(l)	-1491202	191.958	164.31	24.00			-36.28207		298 - 600	[5]
			190.79						600 - 3000	[5]
Gasses										
O_2(g)	0	205.04	26.924	16.97868	-79.16166		2.29329		298-1000	[5]
	”	”	89.681	-1.44745	-4126.537	95.80396	-186.82686		298-1000	[5]

$Cp(Jmol^{-1}K^{-1}) = a + b(10^{-3})T + cT^{-0.5} + d(10^3)T^{-1} + e(10^5)T^{-2} + f(10^7)T^{-3}$

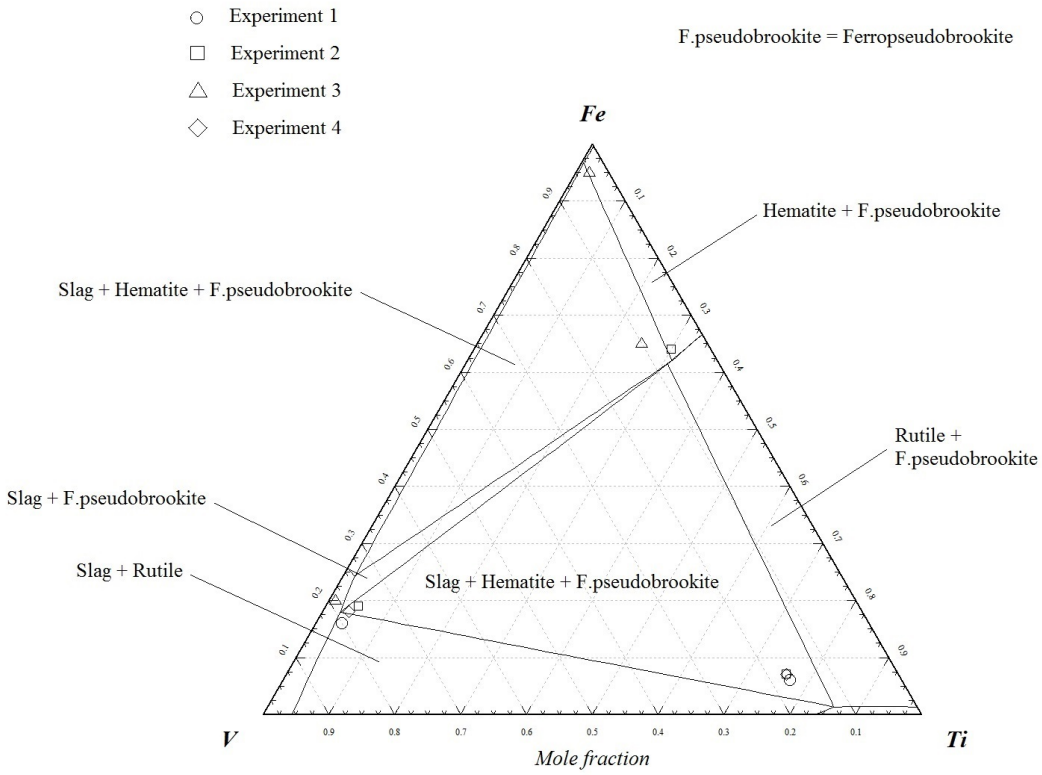

Figure 6: Isothermal section of the Fe-T-V-O system in air (pO_2 = 0.21 atm) at 1000 °C compared with present experimental works.

Table 5: Calculated invariant reactions and phase transitions in the Fe−Ti−V−O system in air from optimized parameters.

V mole %	Fe mole %	Temperature °C	Type of invariant	Equilibrium solid phases
94	4	649	Eutectic	V_2O_5, $Fe_2V_4O_{13}$, rutile
92	6	674	Peritectic	$FeVO_4$, $Fe_2V_4O_{13}$, rutile
81	17	819	Eutectic	$FeVO_4$, Ferropseudobrookite, rutile
80	18	860	Peritectic	$FeVO_4$, Ferropseudobrookite, hematite

The composition of the ferropseudobrookite solid solution was accurately described when in equilibrium with the slag and rutile solid solution. However, when the ferropseudobrookite solid solution was in equilibrium with the slag and hematite solid solution, the simple polynomial model failed to reproduce the ratio of Fe to Ti accurately. This can be corrected by including Fe_2O_3(s) and TiO_2(s) in the model of ferropseudobrookite solid solution, and developing the model within the framework of the CEF. However, more solubility and occupancy data of the ferropseudobrookite solid solution in the lower order Fe-Ti-O system under oxidising conditions are firstly required.

The optimised parameters related to the Fe-Ti-O system were finally cross-checked by back-calculating the lower order Fe-Ti-O phase diagram under oxidizing conditions and comparing to the available Fe-Ti-O phase diagram ($pO_2 = 0.21$ atm) in FactSage.

In the phase diagram estimated with FactSage (Figure 12a) there are three solid compounds, Fe_2TiO_5(s), rutile and hematite, and one slag phase. It is stated in the documentation of the FtOxid database that the slag phase of the Fe-Ti-O system has not been evaluated under oxidising conditions (see section 2). There is also an area where a transition of hematite to pure spinel/magnetite takes place. Supported by the experimental results from this study, it is our finding that the phase diagram estimated in FactSage is incomplete and does not show all solution phases in detail

Conversely, the phases shown in Figure 12b have been evaluated in this study from the assessment of the Fe-Ti-V-O system in air. Clearly better estimations on TiO_2(s) and Fe_2O_3(s) solubility, and slag mixing properties can be made

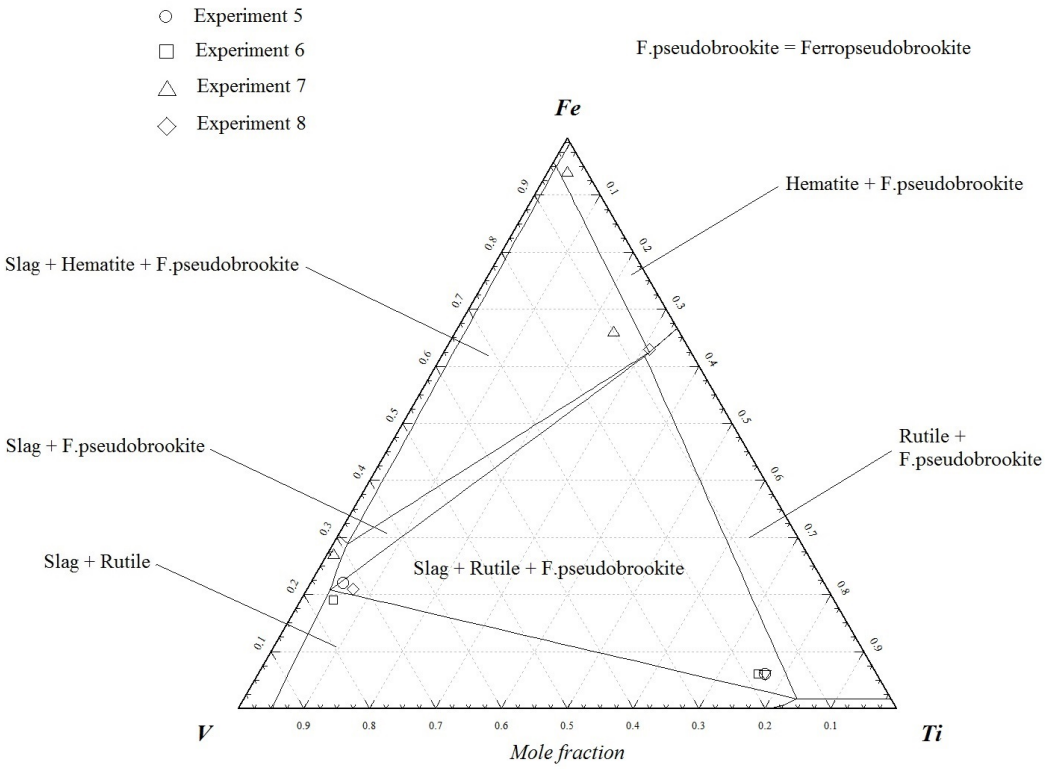

Figure 7: Isothermal section of the Fe-T-V-O system in air (pO_2 = 0.21 atm) at 1100 °C compared with present experimental works.

from the assessed parameters of this study. Furthermore, the decomposition temperature of Fe_2TiO_5(s) into Fe_2O_3(s) and TiO_2(s) in Figure 12b corresponds significantly better with the reported temperature of 565±15 °C. Although the calculated phase diagram shown in Figure 12b describes the slag, hematite and rutile solid solutions better, it is still incomplete due to the shortage of occupancy data on the ferropseudobrookite and spinel solid solution.

For instance, in our calculations it was assumed that the solid state transition of hematite to spinel or magnetite does not take place. In other words, spinel was not included in the final calculation and the melting point of pure hematite shown in Figure 12b may not be entirely correct. The calculated liquidus and solidus compositions above 1400 °C are from extrapolation of the model equations and in reality, a transition is likely to occur at some temperature above 1400 °C. Moreover, some titanium is also likely to report to spinel, which in turn can influence the transition temperature of this hematite solid solution to spinel. More experimental data are required to substantiate such an assumption.

7. Conclusions

In this investigation, phase equilibria were experimentally investigated in the Fe-Ti-V-O system coupled with a thermodynamic evaluation. A set of plausible starting experimental compositions was determined at 1000 °C, 1100 °C, 1200 °C, 1300 °C and 1400 °C by means of extrapolation and interpolation with thermodynamic parameters obtained from the thermodynamically assessed Fe-V-O, Ti-V-O and Fe-Ti-O systems. The Gibbs phase rule was applied meticulously to avoid redundant experiments. Polished and coated samples were analysed with EPMA and SEM-EDS. However, the results from SEM-EDS were compromised by the overlapping of the X-ray emission peaks of V and Ti. The results indicated that Ti dissolution in the V-O slag was encouraged by Fe dissolution. This was significant, given that very little Ti dissolved in the slag phase of the Ti-V-O system in air at similar temperatures. Furthermore, it was observed that a small amount of Fe_2O_3(s) and V_2O_5 dissolved in the ferropseudobrookite phase.

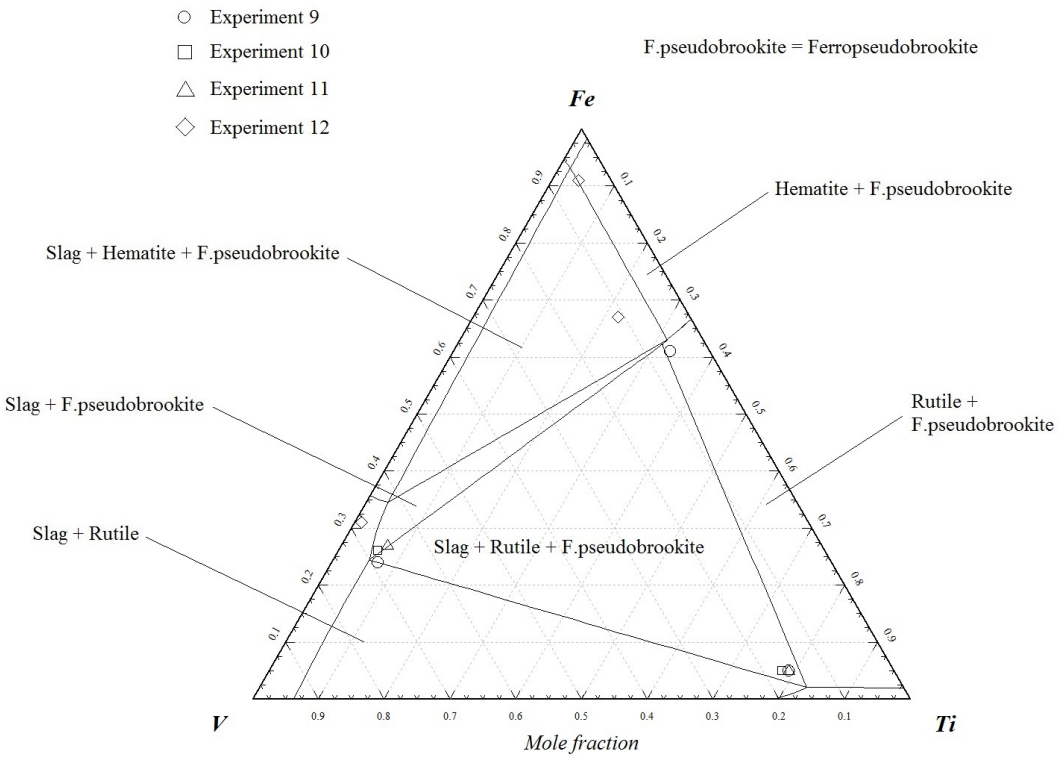

Figure 8: Isothermal section of the Fe-T-V-O system in air (pO_2 = 0.21 atm) at 1200 °C compared with present experimental works.

The modified quasichemical model was used to describe the properties of the liquid. The liquidus was successfully reproduced by optimizing only parameters applicable to the Fe-Ti-O system. The optimized parameters indicated strong short-range ordering near the congruent melting point of ferropseudobrookite. It should be pointed out that the domination of the ferropseudobrookite associate in the present work is calculated based on the mathematical expression of the Gibbs energy functions, instead of being experimentally confirmed. This also means that the congruent melting point of the ferropseudobrookite solid solution was not experimentally determined, but that the best agreement between experimental and calculated results was achieved when such an assumption was made.

The dissolution of TiO_2 and V_2O_5 in the hematite phase and V_2O_5 and Fe_2O_3 in the rutile phase was developed within the framework of the compound energy formalism. Both models were derived and expanded from the Fe-V-O, Ti-V-O and Fe-Ti-O systems. The dissolution of V_2O_5 in the ferropseudobrookite phase was described with a simple polynomial model. A set of self-consistent thermodynamic parameters was achieved on the basis of the optimisation considering data from present experiments. A set of calculated isothermal sections with superimposed experimental data and liquidus projection was provided, together with calculated temperatures and compositions of invariant reactions. In addition, a Fe-Ti-O phase diagram in air was estimated using optimised parameters and compared to the phase diagram available in FactSage.

Finally, it is our recommendation that more experimental be done under reducing conditions to extend the database of the present study to make it applicable for real processes such as the extraction of vanadium from titaniferous ores, and other industrial applications based on the Fe-Ti-V-O system.

8. Acknowledgements

This work was supported financially by the Glencore Chair in Pyrometallurgical Modelling at the University of Pretoria. We would also like to express gratitude to Aalto University, School of chemical Engineering for lending their

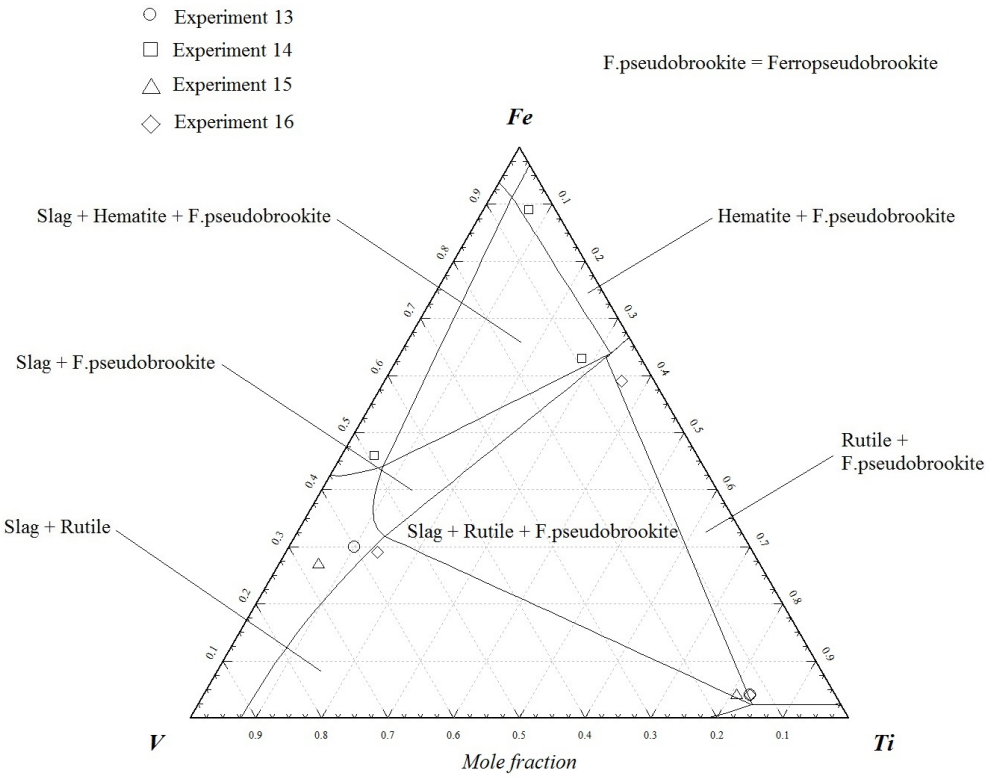

Figure 9: Isothermal section of the Fe-T-V-O system in air (pO_2 = 0.21 atm) at 1300 °C compared with present experimental works.

facilities to carry out experimental work. The authors of this work would further like to thank Dr Christian Reinke at the University of Johannesburg for his assistance and cooperation with EPMA work.

A. Supplementary information

The raw data required to reproduce these findings are available to download from [https://data.mendeley.com/submissions/evise/edit/nvpgs2vjmr?submission_id=S0364-5916(18)30217-7&token=6bc0021a-85ab-4ea8-85c1-4f774cda067e]. The processed data required to reproduce these findings are available to download from [https://data.mendeley.com/submissions/evise/edit/nvpgs2vjmr?submission_id=S0364-5916(18)30217-7&token=6bc0021a-85ab-4ea8-85c1-4f774cda067e].

References

[1] W. Malan, G. Akdogan, P. Taskinen, J. Hamuyuni, J. Zietsman, Phase equilibria and thermodynamic evaluation of Fe-V-O system in air, CALPHAD: Computer Coupling of Phase Diagrams and Thermochemistry 63 (2018) 12–23, URL https://doi.org/10.1016/j.calphad.2018.08.003.

[2] W. Malan, G. Akdogan, P. Taskinen, J. Hamuyuni, J. Zietsman, Phase equilibria and thermodynamic evaluation of Ti-V-O system in air, CALPHAD: Computer Coupling of Phase Diagrams and Thermochemistry 63 (2018) 220–228, URL https://doi.org/10.1016/j.calphad.2018.10.006.

[3] G. Erikson, A. Pelton, Critical evaluation and optimization of the thermodynamic properties and phase diagrams of the $MnO-TiO_2$, $MgO-TiO_2$, $FeO-TiO_2$, $Ti_2O_3-TiO_2$, Na_2O-TiO_2 and K_2O-TiO_2 systems, Metallurgical Transactions B 24 (B) (1993) 795–805, URL http://dx.doi.org/10.1007/BF02663140.

[4] G. Erikson, A. Pelton, E. Woermann, A. Ender, Measurement and thermodynamic evaluation of phase equilibria in the Fe-Ti-O system, Berichte Der Bunsengesellshaft 100 (11) (1996) 1839–1849, URL http://dx.doi.org/10.1002/bbpc.19961001114.

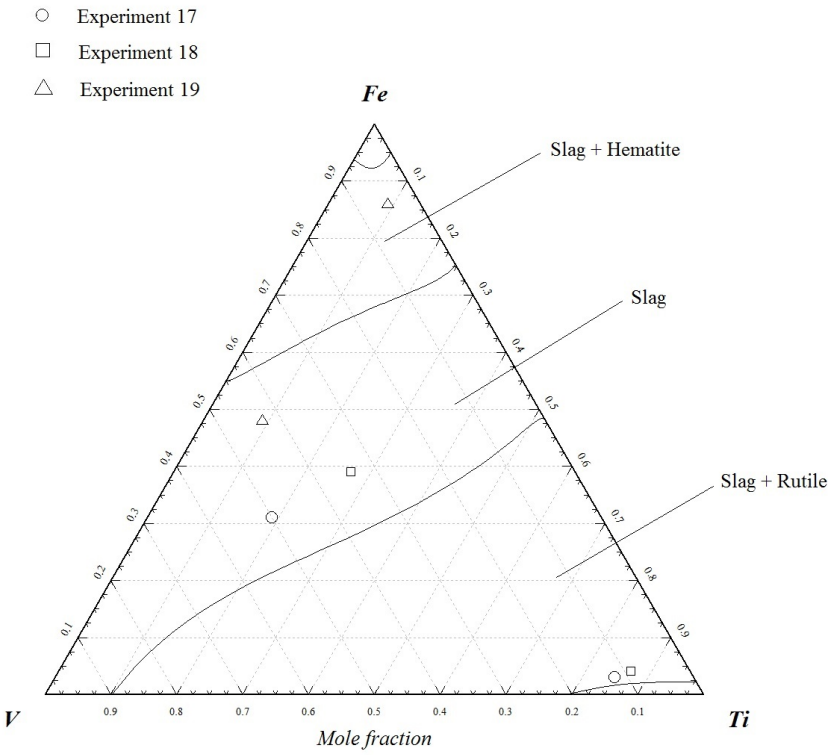

Figure 10: Isothermal section of the Fe-T-V-O system in air (pO_2 = 0.21 atm) at 1400 °C compared with present experimental works.

[5] C. Bale, E.Belisle, P. Chartand, S. Decterov, G. Eriksson, K. Hack, I. Jung, Y. Kang, J. Melancon, A. Pelton, C. Robelin, S. Petersen, FactSage thermochemical software and databases, 2010-2016, CALPHAD: Computer Coupling of Phase Diagrams and Thermochemistry 54 (2) (2016) 35–53, URL https://doi.org/10.1016/j.calphad.2016.05.002.

[6] A. A. Fotiev, L. L. Surat, A. I. Tret'yakov, Compatibility relations in the $FeO_3-TiO_2-V_2O_5$ system, Russian Journal of Inorganic Chemistry 26 (5) (1981) 1377–1382.

[7] E. Jak, P. Hayes, Phase equilibria determination in complex slag systems, Mineral Processing and Extractive Metalllurgy: Transactions of the Institutions of Mining and Metallurgy 117 (1) (2008) 1–17, URL http://dx.doi.org/10.1179/174328508X272344.

[8] H. Lukas, S. Fries, B. Sundman, Computational thermodynamics, the Calphad method, Cambridge University press, Cambridge, UK, 2007.

[9] W. Steinberg, W. Geyser, The history and development of the pyrometallurgical processes at Evraz Highveld Steel & Vanadium, in: R. Jones, P. Hoed (Eds.), Southern African Institute of Mining and Metallurgy, 1034–1045, 2011.

[10] S. Haggerty, D. Lindsley, Stability of the pseudobrookite (Fe_2TiO_6) ferropseudobrookite (Fe_2TiO_5) series, Carnegie Inst. Wash. Year Book 68 (1970) 247–249.

[11] A. Navrotsky, Thermodynamics of formation of some compounds with the pseudobrookite structure and of the $FeTi_2O_5-Ti_3O_5$ solid solution series, American Mineralogist 320 (3-4) (1975) 249–256.

[12] W. Guo, S. Malus, D. Ryan, Z. Altounian, Crystal structure and cation distributions in the $FeTi_2O_5$-Fe_2TiO_5 solid solution series, Journal of Physics: Condensed Matter 11 (4) (1999) 413–419, URL https://doi.org/10.1016/j.pnsc.2013.06.012.

[13] R. Robert, CRC Handbook of Chemistry and Physics, vol. 62, Boca Raton, FL: CRC Press, Cambridge, UK, URL ISBN0-8493-0462-8, 1981.

[14] C. Merlet, An Accurate Computer Correction Program for Quantitative Electron Probe Microanalysis, Mikrochim. Acta 114/115 (1994) 363–376.

[15] M. Koretsky, Engineering and chemical thermodynamics, vol. 1, John Wiley and Sons, Inc., 111 River Street, Hoboken, NJ 07030, 2004.

[16] A. Pelton, M. Blander, Thermodynamic Analysis of Ordered Liquid Solutions by a Modified Quasi-Chemical Approach - Application to Silicate Slags, Met. Trans. B 17B.

[17] A. Pelton, M. Blander, Thermodynamic Analysis of Binary-Liquid Silicates and Prediction of Ternary Solution Properties by Modified Quasi-Chemical Equations, Geochim. Cosmochim. Acta 51 (1987) 85–95.

[18] W. Xie, N.Wang, Z. Qiao, Z. Cao, Thermodynamic assessment of the PbO - V_2O_5 system, CALPHAD: Computer Coupling of Phase Diagrams and Thermochemistry URL http://dx.doi.org/10.1016/j.calphad.2016.04.005.

[19] P. Hudon, I. Jung, Critical evaluation and thermodynamic optimization of the $CaO-P_2O_5$ system, Metallurgical and Materials Transactions

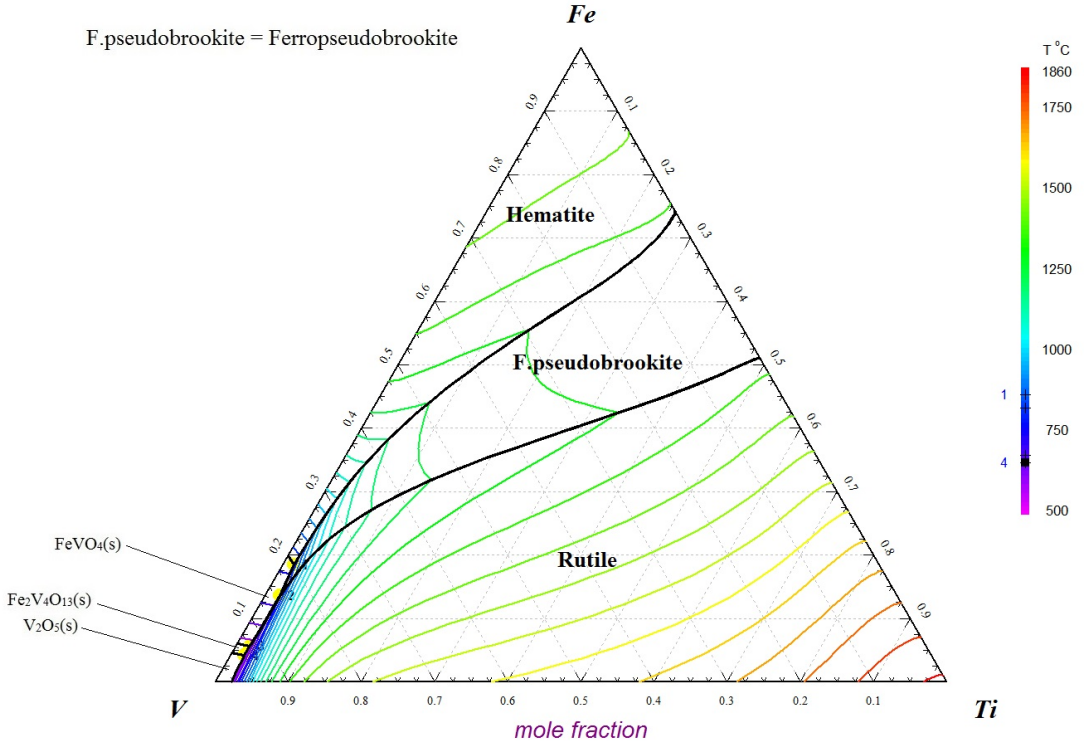

Figure 11: Calculated liquidus projection of the Fe-Ti-V-O system in air ($pO2$ = 0.21 atm) from optimised parameters.

B 46 (B) (2014) 494–522.

[20] M. Rahman, P. Hudon, I. Jung, A coupled experimental study and thermodynamic modelling of the $SiO_2-P_2O_5$ system, Metallurgical and Materials Transactions B 44 (B) (2013) 837–852.

[21] Y. Kawakita, H. Nakashima, S. Yoshioka, S. Takeda, K.Maruyama, M. Inui, K. Tamura, Local structures of liquid and vitreous V_2O_5 and P_2O_5, Journal of Physics and Chemistry of Solids 60 (1999) 1483 – 1486, URL http://dx.doi.org/S0022-3697(99)00148-1.

[22] S. A. Degterov, E. Jak, P. Hayes, A. D. Pelton, Experimental study of phase equilibria and thermodynamic optimization of the Fe-Zn-O system, Metallurgical and Materials Transactions B 32 (B) (2001) 643–657, URL http://dx.doi.org/10.1007/s11663-001-0119-2.

[23] Y. Kang, I. Jung, H. Lee, Critical evaluation and optimization of the MnO-$TiO_2-Ti_2O_3$ system, CALPHAD: Computer Coupling of Phase Diagrams and Thermochemistry 30 (2006) 235–247, URL http://dx.doi.org/10.1016/j.calphad.2006.05.001.

[24] N. Wang, Critical evaluation and thermodynamic assessment of the $CaO-MgO-V_2O_5$ system, M.sc. thesis, University of Science and Technology, Beijing, 2015.

[25] V. Prostakova, J.Chen, E.Jak, S. Decterov, Experimental investigation and thermodynamic modelling of the ($NiO+CaO+SiO_2$) and ($NiO+CaO+MgO+SiO_2$), J. Chem. Thermodynamics 86 (B) (2015) 130–142, URL http://dx.doi.org/10.1016/j.jct.2015.01.017.

[26] C. Bale, P.Chartrand, S. Degterov, G.Eriksson, K.Hack, R. Mahfoud, J. Melancon, A. Pelton, S.Petersen, FactSage thermochemical software and databases, CALPHAD: Computer Coupling of Phase Diagrams and Thermochemistry 26 (2) (2002) 189–228, URL http://dx.doi.org/10.1016/S0364-5916(02)00035-4.

[27] I. Jung, S. Deceterov, A. Pelton, Critical thermodynamic optimization of the Fe-Mg-O system, Journal of Physics and Chemistry of Solids 65 (1) (2004) 1683–1695, URL http://dx.doi.org/10.1016/j.jpcs.2004.04.005.

[28] W. Zhang, M. Chen, Thermodynamic modelling of the Co-Fe-O system, CALPHAD: Computer Coupling of Phase Diagrams and Thermochemistry 41 (1) (2013) 76–88, URL http://dx.doi.org/10.1016/j.calphad.2013.02.002.

[29] M. Hillert, L. Staffansson, The Regular Solution Model for Stoichiometric Phases and Ionic Melts., Acta Chem. Scand. 24 (1970) 3618–3626,

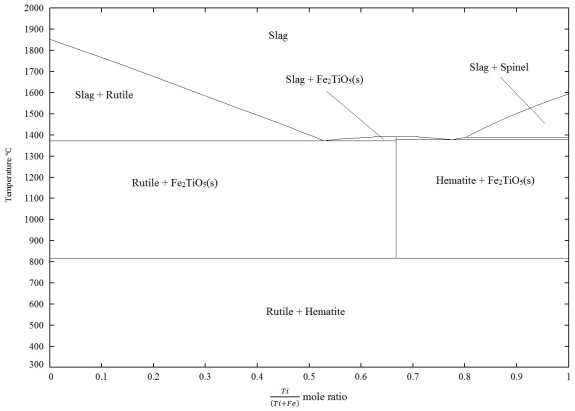

(a) The Fe-Ti-O phase diagram in air estimated with FactSage [5].

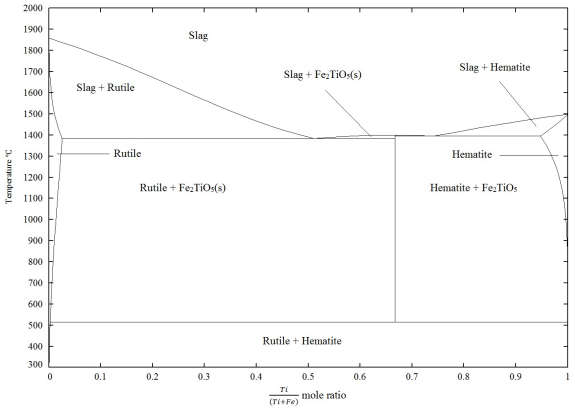

(b) The calculated Fe-Ti-O phase diagrams in air using optimised parameters of this study.

Figure 12: Comparing the calculated Fe-Ti-O phase diagram in air ($pO_2 = 0.21$ atm) from this study to the phase diagram available in FactSage.

URL http://dx.doi.org/10.3891/acta.chem.scand.24-3618.

[30] B. Sundman, J. Agren, A regular solution model for phases with several components and sublattices, suitable for computer applications., Journal of Physics and Chemistry of Solids 42 (4) (1981) 297–301, URL http://dx.doi.org/10.1016/0022-3697(81)90144-X.

[31] M. Hillert, The compound energy formalism, Journal of Alloys and Compounds 320 (2) (2001) 161–176, URL https://doi.org/10.1016/S0925-8388(00)01481-X.

[32] J. Wittke, Solubility of Iron in TiO_2 (Rutile), Journal of the American Ceramic Society 50 (11) (1967) 586–588, URL https://doi.org/10.1111/j.1151-2916.1967.tb15004.x.

[33] M. Cancarevic, M. Zinkevich, F. Aldinger, Thermodynamic description of the Ti-O system using the associate model for the liquid phase, CALPHAD: Computer Coupling of Phase Diagrams and Thermochemistry 31 (2007) 330–342, URL http://dx.doi.org/10.1016/j.calphad.2007.01.009.